Materials Advances

Accepted Manuscript

This article can be cited before page numbers have been issued, to do this please use: Z. Tang and O. Rius-Ayra, *Mater. Adv.*, 2026, DOI: 10.1039/D6MA00298F.

ROYAL SOCIETY OF CHEMISTRY

rsc.li/materials-advances

View Article Online
DOI: 10.1039/D6MA00298F

3D-Printed Superhydrophobic Copper Mesh for Oil/Water Separation and Microplastics Capture

Zhe Tang, Oriol Rius-Ayra*

CPCM, Department of Materials Science and Physical Chemistry, University of Barcelona, Martí i Franquès 1-10, 08028 Barcelona, Spain

Abstract: This study develops a robust superhydrophobic and superoleophilic copper mesh via a facile two-step process involving chemical etching and lauric acid modification. The resulting surface possesses a hierarchical micro/nanoscale roughness and an ultra-low-energy coating, yielding a water contact angle of 160° and good oil affinity. This engineered wettability enables the mesh to achieve separation efficiencies exceeding 95% for various oil-water mixtures. Furthermore, the material demonstrates an excellent capability for removing polypropylene (PP) and high-density polyethylene (HDPE) microplastics, with efficiencies above 94% at moderate concentrations, via synergistic hydrophobic interactions. Remarkably, the integration of a trace oil phase (e.g., hexane) was found to further enhance microplastic capture by acting as a hydrophobic bridge. The mesh also exhibits high chemical stability across a wide pH range (1-14) and

View Article Online
DOI: 10.1039/D6MA00298F

maintains consistent performance over multiple operational cycles. With its multifunctional performance, straightforward fabrication, and proven stability, this copper mesh presents a promising and practical material for advanced applications in oily wastewater treatment and complex water remediation.

Keywords: Nanostructured material, copper, lauric acid, superhydrophobicity, wetting.

1. Introduction

The escalating challenges of marine and freshwater pollution, particularly from oil spills and microplastic contamination, pose significant threats to aquatic ecosystems and human health[1]. These pollutants originate from diverse sources including industrial wastewater discharge, offshore oil operations, and degradation of plastic products, creating an urgent need for efficient and environmentally friendly separation technologies[2,3].

Traditional methods for oil-water separation such as gravity separation, air flotation, and centrifugation face limitations including moderate efficiency, high energy consumption, and potential secondary pollution[4,5]. Similarly, conventional microplastic removal techniques primarily relying on filtration and adsorption often struggle to achieve simultaneous and efficient separation of both oil and microplastics[6,7]. Recently, materials with special wettability have emerged as promising solutions to these challenges, with superhydrophobic/superoleophilic materials showing particular potential due to their selective affinity for oil while completely repelling water[8].

View Article Online
DOI: 10.1039/D6MA00298F

Superhydrophobic surfaces, characterized by water contact angles (WCA) exceeding 150° and sliding angles below 10°, have attracted significant scientific interest due to their unique wetting properties and wide-ranging applications[9]. This extreme water repellency arises from the synergistic combination of micro/nanoscale hierarchical structures and low surface energy chemical modifications. When properly engineered, these surfaces can trap air pockets within their textured morphology, forming a composite solid-air-liquid interface that prevents water droplet penetration[10].

The pursuit of superhydrophobicity has led to the development of various surface modification strategies employing low-surface-energy materials. Among these, fatty acids - particularly lauric acid - have emerged as promising candidates for creating superhydrophobic coatings on metal substrates[11–13]. Lauric acid, a saturated fatty acid containing a 12-carbon alkyl chain, possesses inherent hydrophobicity and can coordinate with metal surfaces through its carboxyl group. This interaction facilitates the self-assembly of organic layers with densely packed alkyl chains outward, effectively reducing surface energy while creating the necessary surface roughness for superhydrophobicity[14]. Among metal substrates, copper mesh stands out due to its low cost, easy processability, and excellent mechanical properties, making it an ideal base material for separation applications[15].

The practical applications of superhydrophobic materials span multiple industrial sectors, with recent focus expanding to environmental remediation. In oil-water separation, their unique superhydrophobic/superoleophilic characteristics enable selective oil absorption while completely repelling water, making them ideal for addressing oil spill incidents and industrial wastewater treatment[16–18]. The integration of superhydrophobic materials with porous substrates like metal meshes has proven particularly effective for continuous oil-water separation processes[19,20].

View Article Online
DOI: 10.1039/D6MA00298F

More recently, emerging research has revealed the capability of superhydrophobic materials to address microplastic pollution in aquatic environments[21–23]. The capture mechanism relies on hydrophobic interactions and van der Waals forces between microplastics and the functionalized surfaces[24]. Current investigations focus on enhancing material sustainability and recyclability, with magnetic functionalization being particularly promising for facilitating post-use recovery[25]. For instance, Ren et al have demonstrated the superhydrophobic magnetic cobalt ferrite particles modified with lauric acid behaved the nearly complete microplastic removal with excellent reusability[26,27].

Despite these advances, the development of copper-based superhydrophobic systems specifically designed for microplastic removal remains insufficiently explored. While copper meshes offer advantages including inherent antimicrobial properties, excellent conductivity, and cost-effectiveness, their potential for addressing microplastic contamination in conjunction with oil-water separation hasn't been fully realized. Most existing studies focus on either oil-water separation or microplastic removal separately, with limited research on materials capable of simultaneously addressing both pollutants[28,29].

To address this research gap, this study presents a facile method for fabricating a superhydrophobic copper mesh through chemical etching and lauric acid modification, demonstrating good performance in oil-water separation and microplastic removal. The developed material exhibits a water contact angle of 160˚ and maintains remarkable stability under various environmental conditions. We systematically evaluated the material's separation efficiency for oil-water mixtures and its capture capability for polypropylene (PP) and high-density polyethylene (HDPE) microplastics. Through comprehensive characterization including XPS and SEM analyses, we investigated the surface chemistry and morphology, and explored the synergistic mechanisms underlying the simultaneous oil-water separation and microplastic removal. This work provides

View Article Online
DOI: 10.1039/D6MA00298F

valuable insights into the development of multifunctional materials for comprehensive water remediation applications.

2. Experimental Procedure

2.1 Fabrication of copper mesh via FFF 3D printing and thermal post-processing

A green part was fabricated via Fused Filament Fabrication (FFF). The printing system comprised a Creality Ender-3 S1 PRO 3D printer equipped with a hardened steel Mk8 nozzle (Brozzl) with a 0.6 mm diameter. The feedstock was a copper-based composite filament (Filamet™ Copper, The Virtual Foundry) supplied with a diameter of 1.75 mm. This filament consisted of 90% copper powder embedded within a polylactic acid (PLA) matrix, which served as a binder during the printing process to shape the metallic structure. To ensure reliable feeding due to the filament's high metal content and stiffness, a filament heater (FilaWarmer, Filament2Print) set at 50 ˚C was installed upstream of the extruder to reduce friction and straighten the filament.

The 3D model was designed in SolidWorks and prepared for printing using UltiMaker Cura 5.2.2 slicing software. The key printing parameters for the green part were set as follows: a nozzle temperature of 215 ˚C, a build plate temperature of 50 ˚C, a printing speed of 30 mm/s, and an infill density of 30%. A brim support structure was used to enhance bed adhesion.

To transform the printed environmentally composite part into a pure, densified metallic structure, a two-step thermal post-processing cycle—debinding and sintering—was essential. This process removed the

View Article Online
DOI: 10.1039/D6MA00298F

temporary PLA binder. For debinding, the 3D-printed part was embedded in refractory alumina powder (Al_2O_3) within a crucible, maintaining a 15 mm clearance from the walls. The crucible was transferred to a furnace where the temperature was gradually raised to 482 ˚C and held for 4 hours to thermally decompose and remove the PLA binder. The system was then cooled to room temperature.

Subsequently, the debound part underwent sintering. It was transferred to a fresh crucible setup, again embedded in alumina powder with the same clearance. The surface was covered with a 25 mm layer of sintering charcoal to create a reducing atmosphere that prevented oxidation. The furnace was heated to 1052 ˚C and maintained at this temperature for 5 hours to facilitate metallic particle fusion and structural consolidation. The sample was then allowed to cool to room temperature within the furnace.

Finally, the sintered copper structure was cleaned to remove surface oxides and processing residues. This involved sequential immersion and sonication in a 10% aqueous H_2SO_4 solution for 1 hour, followed by deionized water for 1 hour, and finally ethanol for 30 minutes.

2.2 Chemical etching treatment on copper mesh

The chemically etched samples were prepared using the 3D-printed and sintered porous copper structures described in Section 2.1 as substrates. The as-sintered copper pieces were first cleaned by immersion in a diluted hydrochloric acid solution (2 mol/L) for 3 minutes to remove the surface oxide layer, followed by ultrasonic cleaning in distilled water for 10 minutes and drying.

etching. The cleaned copper mesh was immersed in an aqueous solution of ferric chloride hexahydrate ($FeCl_3 \cdot 6H_2O$) with a concentration of 2.0 wt.% for 3 hours at room temperature. The etching process is

View Article Online
DOI: 10.1039/D6MA00298F

governed by Eq. (1), where ferric ions (Fe^{3+}) oxidize metallic copper (Cu) to copper ions (Cu^{2+}), while being reduced themselves to ferrous ions (Fe^{2+}). During this process, the strong oxidative etching characteristic of $FeCl_3$ corroded the copper surface, generating a micro/nano-scale rough morphology essential for subsequent superhydrophobic modification. Following etching, the sample was thoroughly rinsed with distilled water for 5 minutes to remove residual etchant and reaction products, then dried in air prior to further process.

$$2FeCl_3(aq) + Cu(s) \rightarrow 2FeCl_2(aq) + CuCl_2(1)$$

2.3 Surface modification on chemical-etched copper

To impart hydrophobic properties to the chemically-etched copper surface, a molecular self-assembly modification was performed using lauric acid. First, a modification solution with a concentration of 0.5 mol/L was prepared by dissolving lauric acid (purity >99%) in absolute ethanol.

The etched copper sample (approximately 0.5 g), prepared according to the method described in Section 2.2 and subsequently cleaned and dried, was placed in a glass container. Then, 5 mL of the aforementioned lauric acid solution was added to ensure the sample was fully immersed. The mixture was left to react at room temperature (25 ˚C) for 24 hours. During this period, lauric acid molecules chemically bonded to the active sites on the copper surface via their carboxyl groups (-COOH), forming a dense and ordered self-assembled monolayer that reduces surface energy. This bonding occurs through a chemical reaction where lauric acid reacts with the copper substrate to form copper laurate, as represented by Eq. (2). The formation of this copper laurate compound results in a dense and ordered self-assembled monolayer that reduces surface energy.

View Article Online
DOI: 10.1039/D6MA00298F

$$2CH_3(CH_2)_{10}COO^- + Cu^{2+} \rightarrow Cu\left(CH_3(CH_2)_{10}COO\right)_2 (2)$$

After the reaction, the supernatant was decanted with the aid of magnetic stirring. To thoroughly remove excess physically adsorb lauric acid molecules, the solid sample was washed four times with absolute ethanol: each time, an appropriate amount of ethanol was added, the sample was briefly dispersed via ultrasonication, and then held at the bottom of the container using a magnet before the wash solution was carefully decanted. Finally, the washed sample was placed in an oven at 55 ˚C for drying and curing for 20 hours to obtain a structurally stable superhydrophobic copper surface. The complete schematic flowchart summarizing the entire fabrication process, encompassing substrate preparation, chemical etching, and surface functionalization, is presented in Fig. 1.

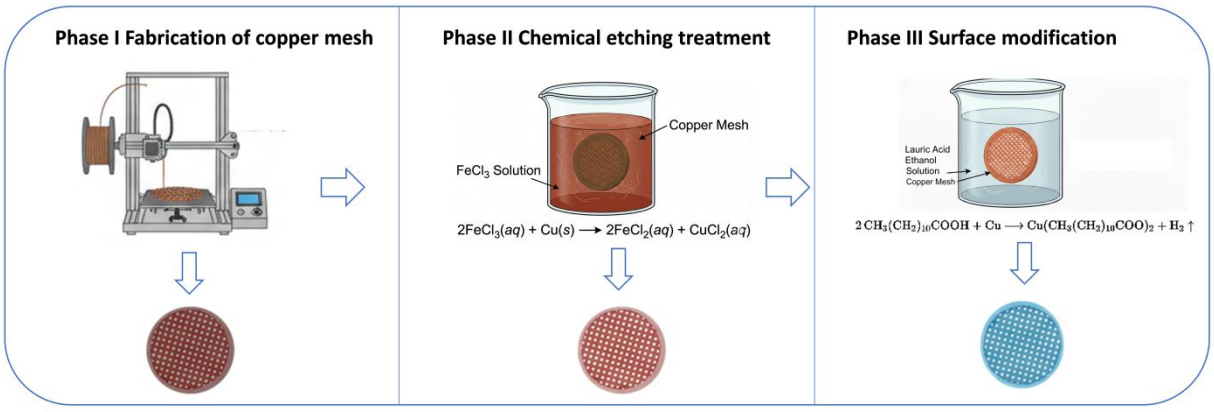

Fig. 1. Schematic flowchart illustrating the fabrication process of the lauric acid-modified superhydrophobic copper mesh, encompassing three main stages: (I) Fabrication of the porous copper substrate via Fused Filament Fabrication (FFF) 3D printing and thermal post-processing (debinding and sintering); (II) Surface

View Article Online
DOI: 10.1039/D6MA00298F

roughening through chemical etching in a $FeCl_3$ solution; (III) Hydrophobic modification via reaction with lauric acid to form a low-surface-energy monolayer

2.4 Oil-water separation

To evaluate the separation performance and application potential of the as-fabricated superhydrophobic copper mesh, hexane was selected as a model organic solvent for oil–water separation tests. In a typical procedure, 20 mL of deionized water was placed in a glass vial, followed by the addition of hexane (stained with Oil Red O) in varying volumes (0.1-5μL). The mixture was then agitated using an orbital shaker at 150 rpm for 10 min to achieve a homogeneous emulsion before separation.

While the hexane-in-water emulsion was continuously agitated, the superhydrophobic copper mesh was immersed into the mixture to enable the in-situ capture and separation of the oil phase. The mesh was subsequently retrieved, and the volume of the residual liquid was recorded. The oil adsorption efficiency (η, %) and adsorption capacity (Q, g/g) were calculated using Eq. (3) and Eq. (4).

$$\eta\ (\%) = \frac{(V_0 - V_r)}{V_0} \times (3)$$

$$Q\ (g/g) = \frac{(m_2 - m_1)}{m_0} (4)$$

where V_0 and V_r represent the initial and residual volumes of hexane (μL), respectively; m_0 denotes the mass of the copper mesh (g); and m_1 and m_2 refer to the masses of the copper mesh before and after oil adsorption (g), respectively.

View Article Online
DOI: 10.1039/D6MA00298F

All experiments were performed in triplicate. The separation efficiency (η) and adsorption capacity (Q) were calculated using Eq. (3) and Eq. (4), respectively. The reported values represent the mean ± standard deviation (SD). After each separation cycle, the mesh was regenerated by rinsing thoroughly with absolute ethanol three times to remove the adsorbed oil, followed by drying in a fume hood for several minutes until complete evaporation of ethanol. This treatment enabled the repeated use of the copper mesh in subsequent oilwater separation tests.

2.5 Microplastics removal

The removal performance of the fabricated superhydrophobic copper mesh was evaluated for the elimination of model microplastics, high-density polyethylene (HDPE) and polypropylene (PP) particles (purchased from Abifor, with sizes in the range of 100–200 μm) using an agitation system. To investigate the potential synergistic effect of an oil phase, parallel experiments were conducted with and without the addition of trace hexane.

For each microplastic type (HDPE or PP), a series of 50 mL aqueous suspensions containing varying masses (5, 10, 15, 20, 25, and 30 mg) were prepared. Subsequently, a 0.5 g sample of the prepared copper mesh was immersed in the suspension. For the experimental group aimed at probing synergy, 20 μL of hexane was added to the suspension using a microliter syringe. Both systems were then agitated at 200 rpm for 60 minutes to enable sufficient contact between the microplastics and the functional surface.

View Article Online
DOI: 10.1039/D6MA00298F

Following the agitation process, the copper mesh was carefully retrieved from the suspension. Any residual water droplets were removed from the mesh using a gentle stream of nitrogen gas. The mesh with adhered microplastics was then dried at 60 ˚C in a fume hood for 2 hours until constant weight was achieved. The mass of microplastics collected on the mesh and any remaining in the suspension were measured. The removal efficiency (η, %) was calculated using Eq. (5).

$$\eta\ (\%) = \frac{(m_0 - m_r)}{m_0} \times\ 100\% (5)$$

where m_0 represents the initial mass of microplastics added to the suspension, and m□ denotes the mass of microplastics remaining in the suspension after the removal process.

For quantification, the remaining suspension after mesh retrieval was filtered through a pre-weighed nylon membrane (0.45 μm pore size). The membrane was dried at 60 °C for 24 h and reweighed to determine the residual microplastic mass. Blank experiments (without the copper mesh) were conducted in parallel to correct for losses to the vial walls, aggregation, and handling errors. All experiments were performed in triplicate, and the reported removal efficiencies are based on the corrected mass balance.

Each microplastic removal test was conducted in triplicate. The removal efficiency (η) was calculated using Eq. (4). Results are expressed as mean ± SD. The procedure was repeated over multiple cycles to assess reusability. Between cycles, the mesh was regenerated by cleaning with absolute ethanol to remove adhered contaminants, followed by drying at room temperature before subsequent use. The coating stability and recyclability were evaluated through twenty consecutive removal cycles for each microplastic type.

View Article Online
DOI: 10.1039/D6MA00298F

3. Characterization techniques

In order to fully understand the role of reactants and the obtained morphology, we used several characterization techniques to determine the structure and chemical composition. In order to determine the chemical composition of the obtained coating, infrared spectroscopy is also used to determine the occurrence of the reaction. For this purpose, Attenuated Total Reflection - Fourier Transform Infrared Spectroscopy (ATR-FTIR) is used in the range of 4000-525 cm^{-1} with a resolution of 4 cm^{-1} (Fourier Transform ABB FTLA). Characterize the surface of superhydrophobic copper mesh on JEOL J-7100 field emission scanning electron microscope (FESEM) to study its detailed morphology, while EDS microanalysis was used to determine the semiquantitative elemental composition in three different positions of each sample. In addition, the chemical composition and bonding states at different depths were analyzed using X-ray photoelectron spectroscopy (XPS). The measurements were performed on an ESFOSCAN & PHI VersaProbe 4 Scanning XPS Microprobe de Physical Electronics (ULVAC-PHI). High-resolution spectra were acquired at the surface and after argon ion sputtering to depths of 5 nm and 10 nm, respectively. Peak deconvolution and analysis of the spectra were conducted using the Multipak.

To evaluate the evolution of surface roughness during the fabrication process, the roughness of three sample types—the pristine copper mesh, the chemically etched mesh, and the final superhydrophobic coating—was characterized on a 1270 × 950 μm^2 area via a white-light confocal microscope (Zeiss Smartproof 5).

We also evaluated the surface wettability through static water contact angle (WCA) measurements performed at room temperature using a Levenhuk digital microscope system. They were determined with 3.5

View Article Online
DOI: 10.1039/D6MA00298F

μL droplets of deionized water and hexane, respectively. To assess pH stability, measurements were also conducted using aqueous solutions across a wide pH range (1, 3, 5, 7, 9, 11 and 13). All contact angles were analyzed via ImageJ software, with reported values representing the mean of three independent measurements performed at different surface locations.

4. Results and discussion

4.1 Surface characterization

The FESEM microscopy analysis was used to show surface morphology of the coating while the EDS was used to determine the semiquantitative composition (Fig. 2): A large number of micron-sized micropapillae are distributed on the surface of the copper mesh (Fig. 2a), especially near the individual pores (Fig. 2b), and a large number of flower-like structures are distributed on each papillae (Fig. 2c-d), and the nanometer-sized thin flakes layered on the surface (Fig. 2e-f), which distributes the micro/nano-complex structure. Therefore, the surface components and micro/nano-composite structures of the copper mesh work together to endow it with unique superhydrophobicity and low adhesion properties.

Microscopic characterization reveals a hierarchical micro/nanostructure on the sample surface. Micron-scale protrusions are densely covered with nano-scale crystalline materials, analogous to the surface morphology of a lotus leaf. This unique architecture significantly enhances the surface contact angle and facilitates the effortless sliding of water droplets.

View Article Online
DOI: 10.1039/D6MA00298F

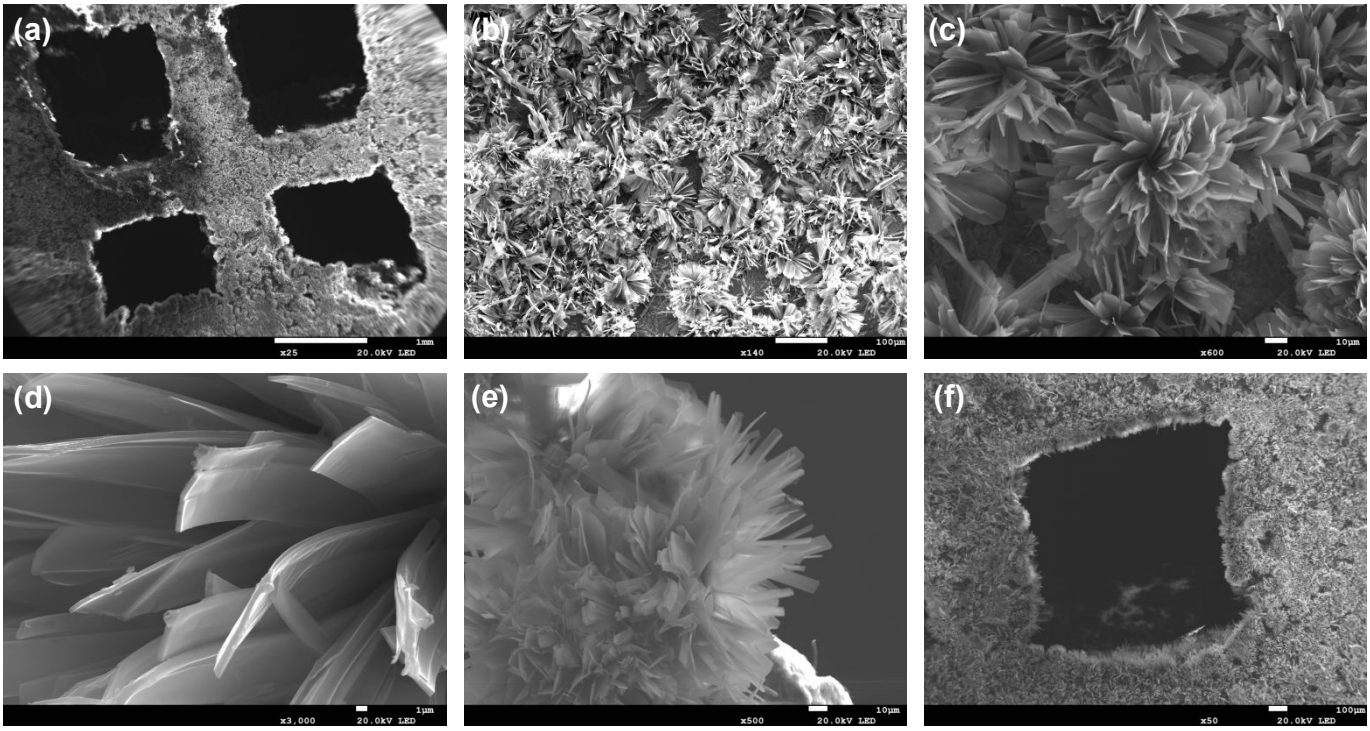

Fig. 2. FESEM images of the copper mesh coating after the surface modification of lauric acid: (a)-(b) poles of copper mesh, (c)-(d) micro-structure of the sample surface, (e)-(f) nanometer-sized layered structures.

In addition, elemental mapping via EDS-SEM reveals the homogeneous distribution of Cu and O across the examined area (Fig. 3a-d), indicating the formation of a thin, uniform surface layer primarily composed of copper, oxygen, and carbon. Furthermore, semi-quantitative EDS analysis (Fig. 3e) yields a Cu:O atomic ratio of approximately 1:4, which is consistent with and verifies the successful chemical formation of copper laurate on the mesh surface. However, since EDS alone cannot confirm chemical bonding, the main evidence for the formation of copper laurate is provided by FTIR (Fig. 4) and XPS (Fig. 5) analyses.

View Article Online
DOI: 10.1039/D6MA00298F

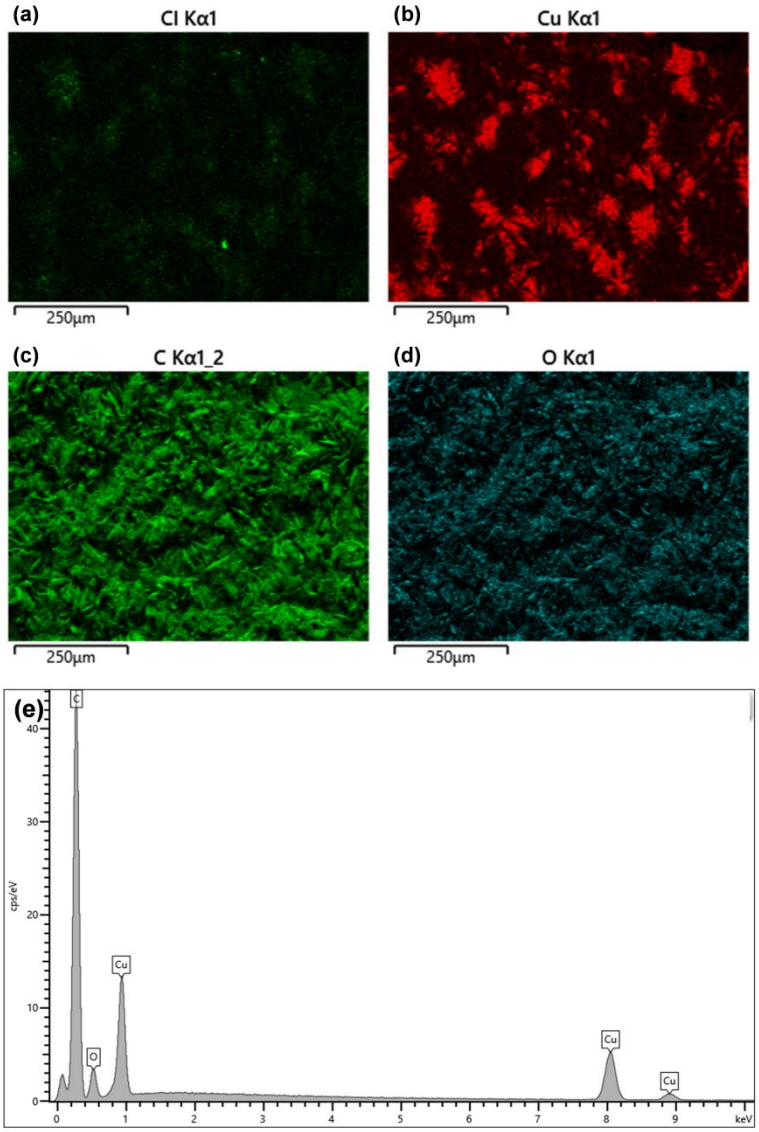

Fig. 3. (a)-(d) characteristic compositional EDS-SEM mapping for the elements C, Cu and O existing on the sample surface, (e) EDS date of specific point of copper mesh and atomic percentage for copper and oxygen atoms from the EDS file.

View Article Online
DOI: 10.1039/D6MA00298F

It should be noted that the 3D-printed copper mesh does not possess an internal porous structure that would allow classical BET porosity analysis. Its surface is highly rough and hierarchical, as evidenced by the FESEM images (Fig. 2), but the oil/water separation mechanism relies on the intrinsic surface wettability (superhydrophobicity/superoleophilicity) and the macroscopic openings of the mesh, rather than on internal porosity. Therefore, conventional measurements of pore size distribution or porosity are not directly applicable to this material.

4.2 Chemical characterization

In order to determine the chemical reactions occurring on the surface of the obtained network, ATR-FTIR and HR-XPS techniques were used to determine the chemical composition of the sample.

Attenuated Total Reflectance - Fourier Transform Infrared (ATR-FTIR) Spectroscopy was carried out in order to obtain information about the chemical bonds adsorbed on the surface of the material. ATR-FTIR spectra of superhydrophobic copper mesh were obtained from 500 cm^{-1} to 3500 cm^{-1} (Fig. 4).

Between about 3000 cm^{-1} and about 2800 cm^{-1}, there are three consecutive signals on the respective spectra of the modified mesh and pure lauric acid attributed to the sp^3 of the alkyl chain of $v_{as}CH_3$, $v_{as}CH_2$, and v_sCH_2-CH_2, respectively. The wild band on the spectra of lauric acid ranging from about 3900 cm^{-1} and about 2300 cm^{-1} correspond to vO-H bond for the hydroxyl group. After the modification of lauric acid, the bond has disappeared in the graph, indicating that the carboxylate functional group of lauric acid (-COOR) have been replaced by the carboxyl group. The difference demonstrates that the chemical reaction from the lauric acid to the copperic laurate has occurred.

View Article Online
DOI: 10.1039/D6MA00298F

The first significantly strong band for the carboxyl group of lauric acid is close to about 1700 cm^{-1} on both spectra corresponding to vC=O[30]. The two bands on the spectra of pure lauric acid are close to 1300 cm^{-1} and 1200 cm^{-1}, respectively, and correspond to different vO-H bonds. The first one corresponds to the carboxyl group of lauric acid, while the second one corresponds to the metal oxide layer on the modified substrate[31]. The signal near 1300 cm^{-1} assigned to vC-O on the spectrum of pure lauric acid is not present on the spectrum of the superhydrophobic substrate. This confirms the formation of carboxylates, where the two C-O bonds become equal due to the electronic resonance between them. Thus, the band at about 1350 cm^{-1} on the spectrum of the prepared lattice is attributed to v_sCOO. The signals on the spectra of both the prepared substrate and the pure acid at about 1450 cm^{-1} are attributed to δCH_2.

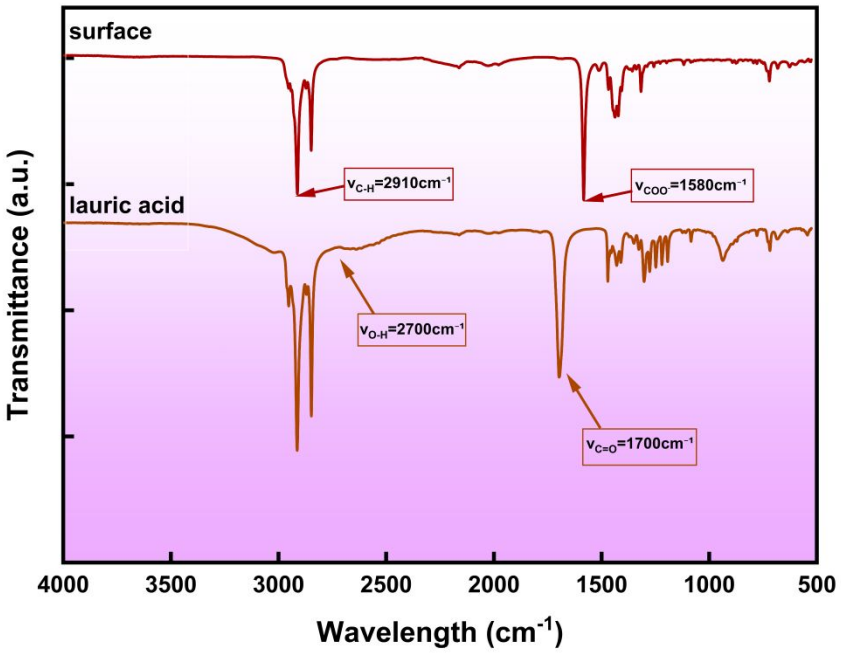

Fig. 4. ATR-FTIR spectra of the superhydrophobic copper mesh and pure lauric acid. The spectrum of the modified mesh confirms the successful formation of copper laurate.

View Article Online
DOI: 10.1039/D6MA00298F

HR-XPS was also used to determine the chemical states of C-1s, O-1s, and Cu-2p at the surface level. The principle of XPS technology is based on the photoelectric effect. When a specific energy of X-ray is irradiated on a solid sample, the inner electrons in the atom can be excited, and the excited photoelectron kinetic energy is detected and analysed by an energy detector. The binding energy corresponding to the electron in the sample can be obtained through the energy conservation equation. Due to the fact that binding energy is the fingerprint information of an element, when the chemical environment around the atom changes, the binding energy of electrons in the inner layer of the element will also change accordingly. Therefore, the chemical binding state of elements can be inferred based on changes in binding energy, which is a qualitative analysis of elements and their chemical states.

For C-1s (Fig. 5a) peaks of copper mesh, there were three different peaks of deconvolutions at approximately 284.8 eV, 286.5 eV, and 288.9 eV, respectively, assigned to C-C/C-H, C-O, and O-C=O bonds, as the carboxylate functional groups[32]. The attribution of C-O and C=O groups to the carboxylate functional group of lauric acid (-COOR) indicates the complete modification of lauric acid on the surface of copper. The dominant peak at 284.8 eV originates from the long alkyl chain of lauric acid, while the carboxylate peak at 288.9 eV confirms the successful formation of copper laurate through the surface modification process[33]. As the sputtering depth increases to 5 nm, the intensity of the C-C/C-H peak decreases substantially, accompanied by a relative increase in the C-O and O-C=O contributions. This transition suggests the gradual attenuation of the intact lauric acid layer and increased exposure of the interfacial region where the carboxylic acid groups coordinate with the copper substrate. At 10 nm depth, the spectrum undergoes a remarkable transformation, with the C 1s signal diminishing to near-background levels. This dramatic reduction indicates that the organic modification layer has been completely penetrated,

View Article Online
DOI: 10.1039/D6MA00298F

revealing the underlying copper substrate[34]. The residual carbon signal at this depth may be attributed to adventitious carbon or deeply embedded reaction products. The depth-dependent chemical composition provides compelling evidence for the successful grafting of lauric acid onto the copper mesh surface, forming a thin, well-defined organic layer that is responsible for the observed superhydrophobic properties. The thickness of this modified layer is estimated to be between 5-10 nm based on the complete disappearance of characteristic carbon signals at 10 nm depth.

In the case of O-1s (Fig. 5b), there were two peaks of deconvolutions at 529.8 and 531.3 eV, corresponding to the Cu-O bond and the C=O bond in carboxylate groups (-COO-), respectively. The presence of the carboxylate peak provides direct evidence for the successful formation of copper laurate through the surface modification process[35]. The depth-dependent analysis shows systematic variations in chemical composition: at the surface (0 nm depth), the carboxylate peak dominates, confirming the complete coverage of lauric acid molecules on the copper mesh. As the sputtering depth increases to 5 nm, the intensity of the Cu-O bond signal significantly enhances, indicating the transition to the interface region. At 10 nm depth, the carboxylate peak nearly disappears, and the spectrum becomes dominated by the Cu-O bond signal, confirming that the organic modification layer has been completely penetrated[36]. This depth profile, consistent with the C 1s analysis, provides compelling evidence for the successful chemical bonding between lauric acid and the copper substrate, with the estimated thickness of the modification layer being approximately 5-10 nm.

Meanwhile, in the case of Cu-2p (Fig. 5c), the spectra exhibit characteristic peaks at binding energies of approximately 932.6 eV (Cu $2p_3/_2$) and 952.5 eV (Cu $2p_1/_2$), accompanied by distinct satellite peaks at around 942.0 eV and 962.3 eV[37]. The presence of these well-defined satellite features, which are

View Article Online
DOI: 10.1039/D6MA00298F

characteristic of Cu^{2+} species, confirms the oxidation state of copper as Cu^{2+} in the surface modification layer. At the surface (0 nm depth), the pronounced satellite structure and the peak positions are consistent with the formation of copper laurate, demonstrating successful chemical coordination between copper atoms and laurate molecules. As the sputtering depth increases to 5 nm, the intensity of the satellite peaks decreases while the main Cu 2p peaks become more dominant, indicating a transition region where both coordinated copper (in copper laurate) and underlying copper oxide species coexist. At 10 nm depth, the satellite features nearly disappear, and the spectrum shows dominant peaks corresponding to Cu^{2+} in copper oxide, confirming that the organic modification layer has been completely penetrated and the bulk substrate region has been reached[38]. This depth-dependent evolution of the Cu 2p spectra, combined with the C 1s and O 1s analyses, provides comprehensive evidence for the formation of a copper laurate surface layer with an estimated thickness of 5-10 nm, where the copper atoms at the interface exist primarily in the Cu^{2+} oxidation state due to their coordination with carboxylate groups from lauric acid.

Taken together, the HR-XPS measurements agree with the ATR-FTIR observations and confirm the chemical formation of copper laurate, which also coincided with the analytical results of EDS analysis and proved the combination of copper laurate.

View Article Online
DOI: 10.1039/D6MA00298F

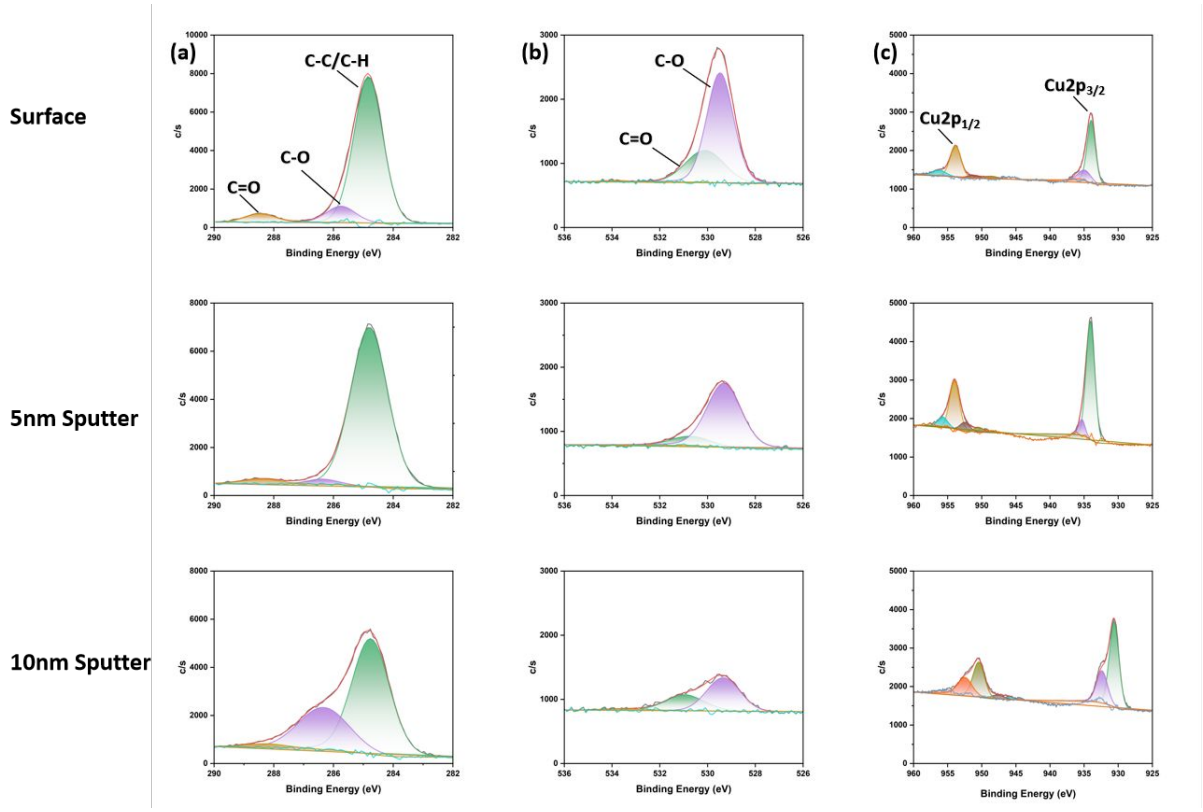

Fig. 5. High-resolution XPS spectra of peaks (a) C1s, (b) O1s and (c) Cu2p generated from the samples at different sputtering depths (0, 5nm and 10nm), respectively.

4.3 Wetting properties

The surface wettability, a critical determinant of superhydrophobicity, was systematically evaluated through water contact angle (WCA) measurements[39]. The lauric acid-modified copper mesh exhibited excellent superhydrophobicity under neutral conditions, with a water contact angle (WCA) of 161 ± 5˚ at pH 7 (Fig. 6a). Under strongly acidic (pH = 1) or alkaline (pH = 13) conditions, the WCA remained above 150˚ (approximately 152˚ and 155˚, respectively), still indicating superhydrophobic behavior. The slight decrease at extreme pH values is attributed to partial protonation of the carboxylate groups or hydrolysis of the lauric

View Article Online
DOI: 10.1039/D6MA00298F

acid layer. High-resolution XPS analysis revealed the presence of C-H groups from lauric acid, which effectively lower the surface energy while maintaining the inherent superoleophilicity essential for oil-water separation applications.

To assess chemical stability, the material was tested with aqueous solutions across a wide pH range of 1, 3, 5, 7, 9, 11 and 13 for 2 hours adjusted using hydrochloric acid (37 wt%) and sodium hydroxide. Remarkably, the prepared surface demonstrated effective droplet repellency not only to pure water but also to corrosive acidic and alkaline solutions, maintaining a WCA consistently above 150˚ throughout the entire pH spectrum (Fig. 6b). The nearly constant contact angles without significant fluctuation indicate good chemical stability in various corrosive liquids. Furthermore, the superhydrophobicity showed no degradation after prolonged air exposure for over two months.

The robust and stable hydrophobic performance primarily originates from the synergistic combination of the engineered surface morphology and the chemical modification. Field-Emission Scanning Electron Microscopy (FESEM) characterization revealed a finely constructed flower-like micro/nano-structure. This hierarchical architecture significantly reduces the actual solid-liquid contact area. When integrated with the low-surface-energy coating formed by lauric acid, it facilitates the stable entrapment of air pockets within the surface nanostructures, thereby promoting the formation of a composite solid-liquid-air interface. This interface is responsible for the observed high WCA.

However, this synergistic effect and the stability of the composite interface can be compromised under extreme chemical conditions. Specifically, exposure to highly acidic or alkaline environments (i.e., very low or high pH) may lead to a measurable decrease in the WCA. The likely explanation for this deviation is the chemical vulnerability of the lauric acid layer. In strong acids, the carboxylate group ($-COO^-$) bonding the

View Article Online
DOI: 10.1039/D6MA00298F

lauric acid to the copper surface could undergo protonation, weakening its adhesion. Conversely, in strong alkaline solutions, the ester bond or the coordination bond between lauric acid and the metal oxide layer on the copper surface may be susceptible to hydrolysis or dissolution. This degradation of the low-surface-energy coating, combined with the potential oxidation or etching of the micro/nano-structured copper substrate itself in harsh pH environments, would diminish the surface's ability to stably trap air. Consequently, the composite interface collapses, leading to an increased solid-liquid contact area and a corresponding decline in hydrophobicity.

The synergistic effect between the multi-scale roughness and hydrophobic terminal groups enables the good and persistent superhydrophobicity that distinguishes it from conventional coatings. These findings demonstrate the material's excellent stability across broad pH ranges and its promising potential as a superhydrophobic coating for various corrosive environments.

View Article Online
DOI: 10.1039/D6MA00298F

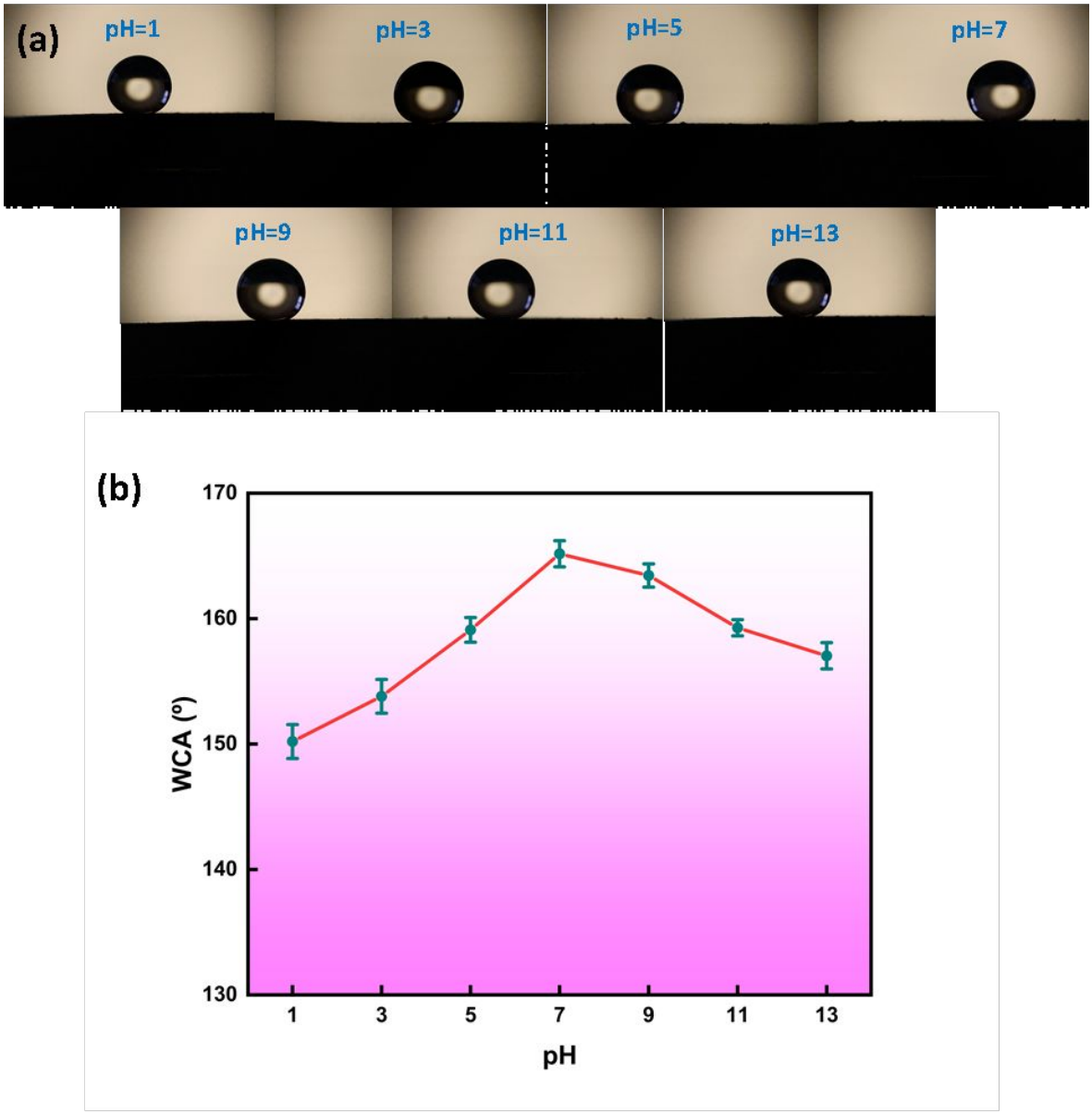

Fig. 6. (a) Photographs of water droplets at different pH values on the superhydrophobic surface. The nearly spherical droplet shapes across the entire pH spectrum visually confirm the persistent non-wetting capability and chemical robustness of the coating under various corrosive conditions. (b) WCAs of the superhydrophobic copper mesh across a wide pH range (1-14). The material maintains a WCA above 150˚ under both acidic and alkaline conditions, demonstrating good chemical stability and effective droplet repellency in corrosive environments.

View Article Online
DOI: 10.1039/D6MA00298F

4.4 Oil/Water separation

Superhydrophobic coatings applied to mesh or porous substrates enable effective oil–water separation, demonstrating significant potential for mitigating marine pollution from oil spills and contributing to the sustainable development of marine ecosystems[40–42]. To evaluate the oil–water separation performance of the prepared copper mesh, hexane was employed as a model organic solvent. The separation process (Fig. 7a), showed that the Oil Red O-stained hexane was rapidly attracted to the copper mesh. The stained area on the water surface diminished over time and was completely adsorbed within 5 minutes. To simulate realistic mixing conditions, an agitation system was employed to homogenize the hexane-water mixtures prior to separation. Different volumes of hexane (0.1-5μL) were added to 20 mL of water and mixed using an orbital shaker operating at 150 rpm for 10 minutes to form a uniform emulsion. This standardized pretreatment ensures reproducible contact between the oil phase and the superhydrophobic surface.

The superhydrophobic copper mesh demonstrated excellent separation capability across a wide range of hexane concentrations (Fig. 7b). At lower hexane volumes (0.1-1 μL), the separation efficiency (η) remained goodly high, reaching up to 99.8%. Although the efficiency gradually decreased with increasing oil concentration, it maintained values above 90% for volumes up to 3.5 μL and still achieved 60.5% even at the highest tested volume of 5 μL.

The observed decrease in removal efficiency with higher oil volumes can be attributed to several interrelated factors. Primarily, the finite adsorption capacity of the superhydrophobic surface becomes a

View Article Online
DOI: 10.1039/D6MA00298F

limiting factor[43]. At low oil concentrations, the hierarchical microstructure provides sufficient active sites and trapped air pockets to effectively capture and separate all incoming oil droplets. However, as the oil volume increases, these sites become saturated. Beyond a critical loading, the surface cannot maintain the stable solid-liquid-air composite interface essential for superhydrophobicity, leading to partial wetting and reduced separation efficiency[44]. Additionally, increased oil concentration alters the dynamics of the oil-water mixture, potentially leading to droplet coalescence and the formation of a more continuous oil phase that is more difficult to separate completely through surface-based capture[45,46].

The adsorption capacity (Q) showed a similar trend, with the highest value of 0.48 g/g observed at 0.5 μL and a gradual decline to 0.35 g/g at 5 μL. These results indicate that the modified copper mesh exhibits high separation performance, particularly at low to moderate oil concentrations, while maintaining functional capacity even under higher loading conditions. The concentration-dependent performance suggests optimal application ranges for the material while demonstrating its robustness across varying contamination levels[47–49].

To further evaluate the applicability of the mesh for more realistic oily wastewater, additional separation tests were conducted using pump oil (viscosity ~150%cSt) under the same experimental conditions (20%mL water, 5%μL oil, 150%rpm agitation). The superhydrophobic copper mesh achieved a separation efficiency of 92%±%3% for pump oil, albeit with a longer complete adsorption time (approximately 15%min) due to the higher viscosity compared to hexane (5%min). These results, summarized in Table 1, confirm that the mesh retains excellent oil/water separation capability even for more viscous oils.

View Article Online
DOI: 10.1039/D6MA00298F

The oil-water separation mechanism is governed by the specific wetting behavior of the superhydrophobic surface in an aqueous environment, as described by the Cassie-Baxter model[50,51]. Upon immersion in water, the hierarchical micro/nano-structures trap a stable, microscale air layer, creating a composite solid-air-liquid interface that prevents water penetration[52,53]. When an oil droplet encounters this surface, the low interfacial tension between oil and the hydrophobic coating, coupled with the capillary forces within the nanostructures, promotes the spontaneous displacement of the trapped air. The oil rapidly wets and infiltrates the textured surface due to its inherent affinity for the low-surface-energy coating, while water is repelled. This selective wetting and capillary-driven penetration enable the effective separation of oil from water[54].

The wetting characteristics dictate the process selectivity[55]. When the material contacts water, a stable air cushion trapped within the micro-roughness forms, causing water droplets to bead up on a composite solid-air-liquid interface and be completely blocked from the mesh pores[56]. In contrast, upon contact with oil, the ultra-low oil-solid interfacial tension allows for instantaneous spreading and complete wetting. Driven by strong capillary forces, the oil phase is rapidly adsorbed and continuously penetrates the mesh[57]. Thus, in a gravity-driven filtration setup, the oil phase passes through unimpeded while the water phase is effectively retained, enabling highly efficient, low-energy, continuous separation[58].

In summary, the developed superhydrophobic copper mesh exhibits high separation efficiency, excellent adsorption capacity, and robust recyclability, making it a promising candidate for treating industrial oily wastewater and supporting environmental remediation.

View Article Online
DOI: 10.1039/D6MA00298F

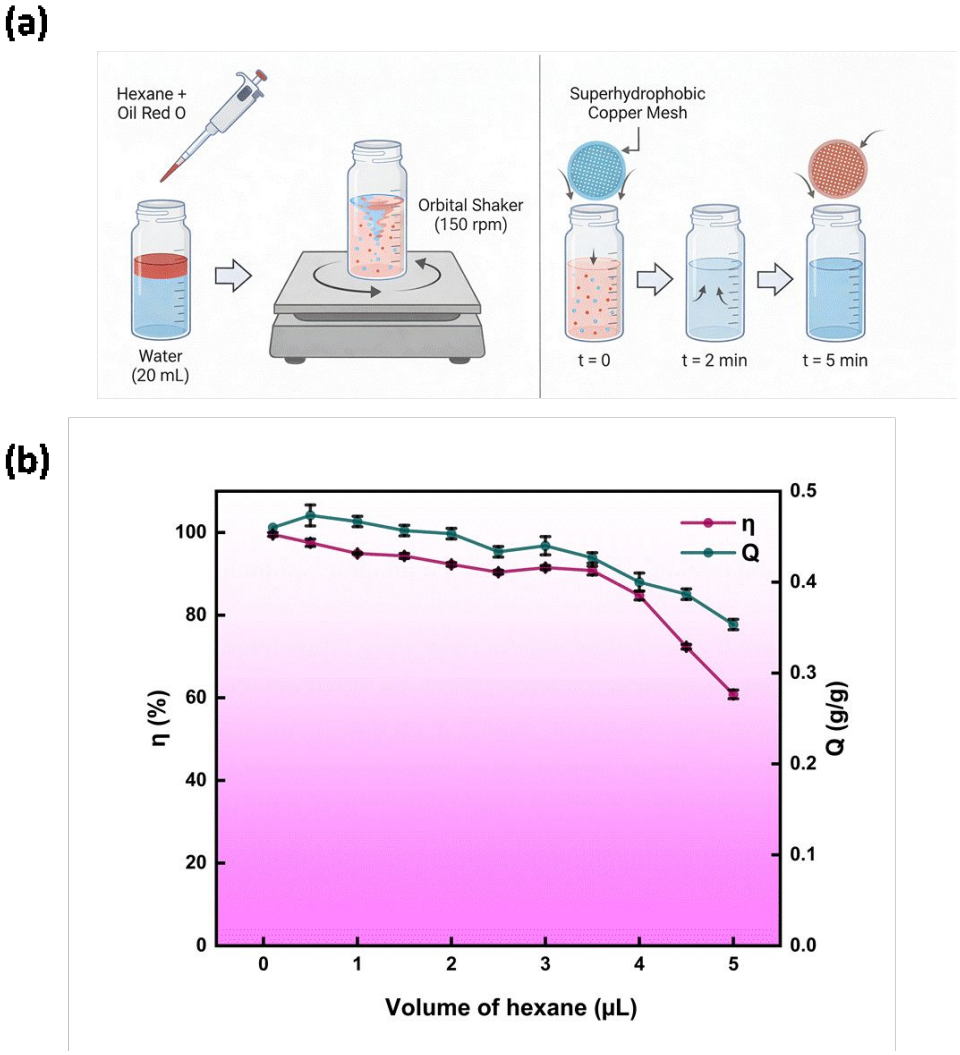

Fig. 7. (a) Oil-water separation process using the superhydrophobic copper mesh. (b) Separation efficiency (η) and adsorption capacity (Q) of the superhydrophobic copper mesh for hexane-water mixtures with varying oil volumes.

Oil type	Viscosity (cSt)	Separation efficiency (%)	Time for complete adsorption (min)
Hexane	~0.3	99 ± 0.5	5
Pump oil	~150	92 ± 3	15

View Article Online
DOI: 10.1039/D6MA00298F

Table.1. Comparison of oil/water separation performance of the superhydrophobic copper mesh for hexane (low viscosity) and pump oil (high viscosity).

4.5 Microplastics removal

The lauric acid-modified superhydrophobic copper mesh demonstrates a high efficiency in selectively capturing and separating polypropylene (PP) and high-density polyethylene (HDPE) microplastic particles from aqueous environments. This remarkable capability originates from its intrinsic superhydrophobic and superoleophilic properties. During the separation process, the water phase is effectively repelled by the air layer trapped within the micro/nanoscale hierarchical structures of the mesh, while the hydrophobic PP and HDPE microplastics are efficiently captured via strong hydrophobic interactions and van der Waals forces[59]. Quantitative removal efficiency analysis confirms the good capture rate of the mesh for both PP and HDPE microplastics. Furthermore, the material exhibits excellent reusability and stability, as it can be easily regenerated through a simple rinsing process with a solvent such as ethanol and maintains high separation performance over multiple operational cycles, underscoring its significant potential for practical application in mitigating microplastic pollution.

Based on the aforementioned principles, the microplastic removal performance of the superhydrophobic copper mesh was systematically evaluated using an agitation system. To comprehensively assess its capability and explore enhancement strategies, two sets of experiments were designed: one to establish the baseline adsorption performance and another to investigate the synergistic effect of an oil phase (Fig. 8a).

View Article Online
DOI: 10.1039/D6MA00298F

In a typical experiment for establishing performance, 50 mL aqueous suspensions containing varying masses (5-30 mg) of either HDPE or PP microplastics were prepared. The superhydrophobic copper mesh (0.5 g) was immersed in the suspension, which was then agitated at 200 rpm for 60 minutes to enable sufficient contact. The removal efficiency demonstrated a clear correlation with microplastic mass (Fig. 8b). For lower mass concentrations (5-15 mg), the mesh achieved good removal efficiencies of 95.2-98.7% for HDPE and 94.8-98.3% for PP. As the microplastic mass increased to 30 mg, the efficiency gradually decreased to 85.6% for HDPE and 84.2% for PP, indicating a saturation effect of the available active sites. The adsorption capacity showed a positive correlation with microplastic mass, reaching maximum values of 0.52 g/g for HDPE and 0.49 g/g for PP at 30 mg loading.

View Article Online
DOI: 10.1039/D6MA00298F

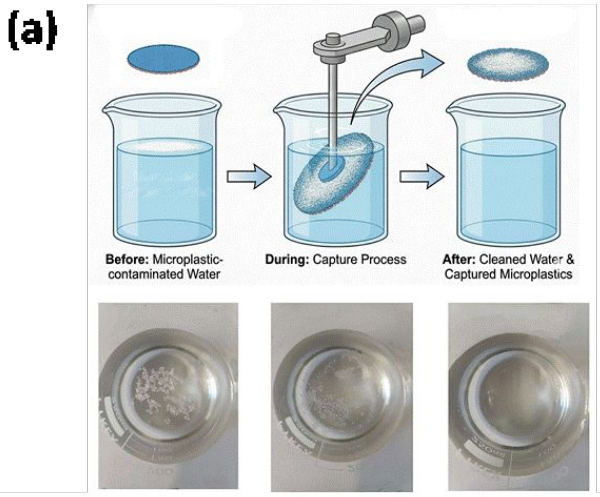

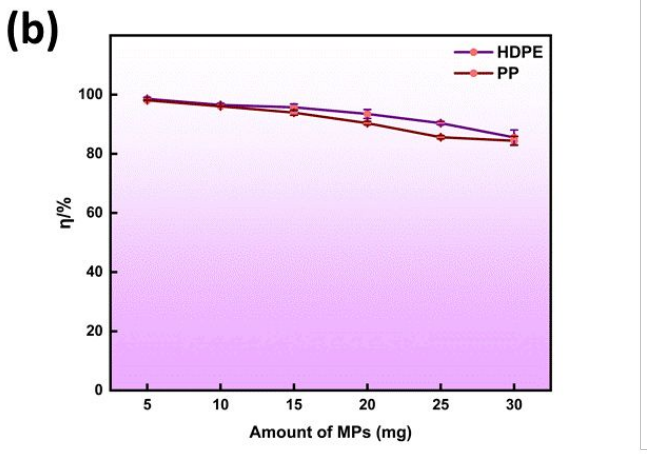

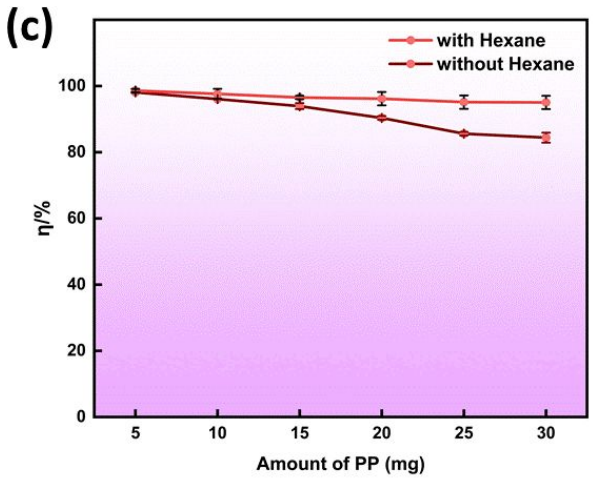

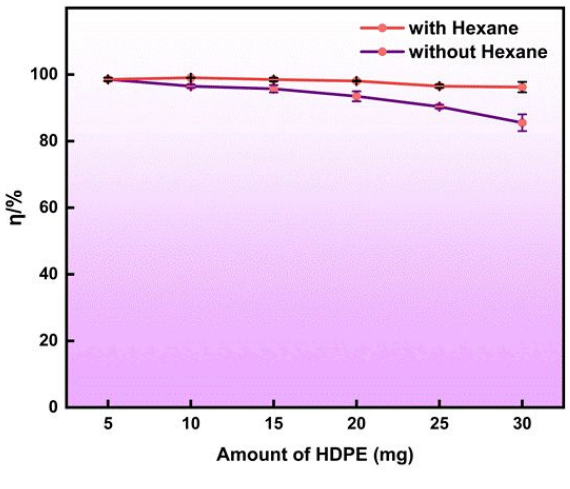

View Article Online
DOI: 10.1039/D6MA00298F

Fig. 8. (a) Schematic of the microplastic removal process using the superhydrophobic copper mesh. (b) Removal efficiency (η) of HDPE and PP microplastics at different initial loadings. (c) Comparison of removal efficiency with and without the addition of hexane, demonstrating the significant synergistic enhancement.

To investigate the hypothesis that a trace oil phase could enhance capture, a parallel set of experiments was conducted with the addition of hexane (20 μL per 50 mL suspension). The introduction of hexane resulted in a marked and consistent improvement in removal efficiency (η) across all tested loadings of both HDPE and PP microplastics compared to the baseline (Fig. 8c). For instance, at a critical mid-range loading of 30 mg, the removal efficiency for PP increased from 84.2% to 95.1%, and for HDPE from 85.6% to 95.7%. This significant enhancement is attributed to a synergistic mechanism where the hexane phase acts as a hydrophobic "bridge". It preferentially wets both the superoleophilic mesh surface and the hydrophobic microplastics, effectively reducing the interfacial energy and facilitating the transfer and attachment of microplastics to the active sites on the mesh. This result confirms that the integration of a minimal oil phase can effectively optimize the system's performance for mitigating microplastic pollution.

Control experiments using an unmodified copper mesh, an etched but non-lauric-acid-modified mesh, and a commercial copper mesh (subjected to the same etching and lauric acid treatment) were performed. The unmodified mesh showed no superhydrophobicity and <5% microplastic removal. The etched-only mesh gave a water contact angle of ~120˚ and ~10% removal. The commercial modified mesh exhibited no superhydrophobicity and 0% removal. These results confirm that both the hierarchical roughness of the 3D-printed mesh and the lauric acid modification are essential for the observed high performance. Moreover,

View Article Online
DOI: 10.1039/D6MA00298F

the synergistic enhancement by a trace oil phase represents a unique feature of our system, distinguishing it from conventional single-function superhydrophobic materials.

Recently, Xiang et al. developed a PEG/MXene@MOF membrane with a stable interlayer spacing for continuous oily wastewater purification, achieving a separation efficiency >99.7% for high-viscosity crude oil emulsions[60]. Gong et al. reported a peony-like $Cu_3(PO_4)_2$/UiO-66-NH_2/PVA composite membrane with an good anti-fouling performance, exhibiting a flux of 4685.96 LMH/bar and a separation efficiency of 99.6%[61]. However, both studies focused exclusively on oil/water separation and did not address microplastic contamination. In contrast, our FFF-printed lauric acid-modified copper mesh not only demonstrates a comparable superhydrophobicity (WCA = 161 ± 5°) and high oil separation efficiency (>99.8%) but also uniquely integrates microplastic capture (removal efficiency up to 98.7% for HDPE and 98.3% for PP) within the same system. Moreover, the 3D printing approach enables the rapid prototyping of hierarchical structures that are difficult to replicate with conventional meshes or planar membranes. These comparisons highlight the distinct advantage of our multifunctional platform for treating complex wastewater containing both oil and microplastics.

Reference	Material	Fabrication method	WCA (°)	OCA (°)	Oil separation efficiency (%)	Microplastic removal efficiency (%)	Adsorption capacity (g/g)	Reusability (cycles)	Durability
This work	3D-printed Cu + lauric acid	FFF + etching + modification	161	0	>99.8 (hexane)	HDPE: 98.7, PP: 98.3	0.52 (MP)	>20	pH 1-14, >150°
[60]	PEG/MXene@MOF membrane	Interfacial assembly	UWOCA >156	–	>99.7 (crude oil)	Not tested	Not reported	Continuous	Anti-fouling
[61]	$Cu_3(PO_4)_2$/UiO-66-NH_2/PVA	Coating	–	–	99.6	Not tested	Not reported	Continuous	Anti-fouling

Table 2. Comparison of key performance parameters of the present 3D-printed superhydrophobic copper mesh with representative materials reported in the literature.

The excellent separation performance can be attributed to the synergistic effect of the mesh's hierarchical structures and surface chemistry. The agitation provided continuous hydrodynamic conditions that enhanced

View Article Online
DOI: 10.1039/D6MA00298F

collision probability between microplastics and the functional surface, while the superhydrophobic interface ensured selective capture through strong hydrophobic interactions. The material maintained stable performance over 20 consecutive cycles with minimal efficiency loss (<5%), confirming its high reusability for continuous microplastic removal applications. During the 20 consecutive cycles, the water contact angle (WCA) decreased only slightly from 161 ± 5° to 158 ± 4° (measured after the final cycle), indicating that no significant fouling by microplastic residues occurred on the mesh surface. A more pronounced decrease would be expected if surface contamination were present.

To assess mechanical durability under dynamic conditions, the mesh was subjected to continuous stirring with microplastic particles (200 rpm, 60 min) for 10 cycles. After this abrasion test, the WCA remained at 152 ± 3°, confirming that the superhydrophobic coating maintains its performance under mild mechanical stress. Furthermore, due to the inherent water repellency of the surface, the presence of dissolved salts (e.g., NaCl) or anionic surfactants (e.g., SDS) in the aqueous phase is not expected to affect the material's performance, as these solutes do not wet or contact the coating.

The enhanced microplastic capture in the presence of a trace oil phase can be rationalized by the extended DLVO theory. The introduction of hexane reduces the interfacial energy between the hydrophobic microplastics and the superoleophilic mesh surface, lowering the energy barrier for adsorption. This thermodynamic driving force, manifested as a reduction in the system's free energy, favors the attachment of microplastics to the oil-wetted surface. The consistent improvement in removal efficiency across all tested loadings (Fig. 8c) further supports this interpretation. While direct spectroscopic evidence of the hydrophobic bridge is challenging to obtain due to the dynamic and non-covalent nature of the interaction, the observed concentration-dependent trends and the well-established principles of hydrophobic attraction provide strong

View Article Online
DOI: 10.1039/D6MA00298F

indirect support for the proposed mechanism. While PP and HDPE particles of 100-200%μm are representative model microplastics, real environmental microplastics exhibit a wide range of sizes, shapes, and polymer types. Future work will extend the study to smaller particles (e.g., <50%μm) and other polymer types such as PET and PVC.

4.7 Mechanism of microplastics removal

The lauric acid-modified superhydrophobic copper mesh achieves simultaneous oil/water separation and microplastic capture through a synergistic multi-mechanism system rooted in interfacial science and surface physicochemistry, rather than a simple combination of independent processes[62].

Its efficacy is fundamentally built upon precise surface properties. The "flower-like" micro-protrusions and nano-sheets constructed on the copper mesh via chemical etching create a natural structural template for entrapping air[63]. Concurrently, the copper laurate generated from the reaction between lauric acid and the substrate forms a dense, orderly, and extremely low-energy molecular layer with outward-facing long alkyl chains[64]. This combination of surface roughness and low surface energy is the origin of the extreme and opposite wetting properties: strong water repellency (superhydrophobicity, with a contact angle of ~160˚) and spontaneous affinity for oils (superoleophilicity, with a contact angle of ~0˚)[65].

For microplastic removal, the mechanism shifts from selective permeation to efficient interfacial adsorption. Both the microplastic particles (e.g., PP and HDPE) and the alkyl chain layer on the material surface are highly hydrophobic. In an aqueous environment, a powerful hydrophobic association occurs

View Article Online
DOI: 10.1039/D6MA00298F

between them to minimize contact with water molecules and reduce the system's overall free energy[66]. This interaction is the dominant force for capture when particles collide with the surface under fluid flow, securing them firmly[67]. Furthermore, the rough surface provides numerous anchoring points that enhance mechanical interlocking, while short-range van der Waals forces contribute additional adsorption stability[68]. The effectiveness of enhancing microplastic attachment through surface superhydrophobization has been demonstrated in related material systems[69].

When confronting complex wastewater containing both oil and microplastics, these two mechanisms exhibit significant synergistic enhancement. The material first selectively captures and enriches the oil phase using its superoleophilicity. Following the "like-dissolves-like" principle, hydrophobic microplastics spontaneously partition from the water phase into the enriched oil phase[70]. Consequently, the microplastics are effectively carried and transported to the material surface by the oil, achieving synchronous and efficient co-removal. This synergy, resulting in superior comprehensive performance for complex wastewater compared to systems treating single pollutants, aligns with the synergistic removal effects observed for oil and microplastics in advanced filtration systems.

The material's long-term practical value is also evidenced by its facile regenerability. Since the adhesion of oil and microplastics primarily relies on physical adsorption and non-covalent interactions, mild regeneration is feasible. Rinsing with a solvent like ethanol effectively dissolves residual oil and disrupts the hydrophobic interaction interface. Subsequent simple drying restores the orderly arrangement of the low-energy alkyl chain layer, allowing the superhydrophobic and superoleophilic properties to be nearly fully recovered, thereby ensuring stable performance over multiple usage cycles.

View Article Online
DOI: 10.1039/D6MA00298F

In summary, this lauric acid-modified copper mesh acts as a multifunctional interfacial material. Its structure-derived extreme wettability enables highly selective oil/water separation, while its surface chemistry-driven strong hydrophobic interactions facilitate effective microplastic capture. In complex polluted environments, these functions work synergistically, making it a promising technological solution for addressing the pressing challenge of composite water pollution.

5. Conclusions

In this study, a superhydrophobic copper mesh was successfully fabricated through a straightforward coating process with lauric acid. Characterization confirmed that the modified surface possesses a flower-like nanostructure composed of copper laurate, endowing the mesh with good superhydrophobicity, as evidenced by a water contact angle (WCA) of 161 ± 5° and an oil contact angle (OCA) of 0 ± 1°. These surface properties enable highly efficient oil–water separation, with the material maintaining a WCA above 150° even after prolonged air exposure, demonstrating good durability.

Separation performance tests revealed that the mesh achieves high separation efficiency (>95%) and notable adsorption capacity (up to 0.48 g/g) for oil–water mixtures across a range of oil concentrations. Furthermore, the superhydrophobic mesh demonstrates excellent microplastic capture capability, achieving removal efficiencies up to 98.7% for HDPE and 98.3% for PP, with a maximum adsorption capacity of 0.52 g/g, primarily through strong hydrophobic interactions. The fabrication method is cost-effective, scalable, and requires no specialized equipment. With its integrated capabilities in oil–water separation and microplastic removal, the developed copper mesh represents a promising and environmentally friendly

View Article Online
DOI: 10.1039/D6MA00298F

material for the treatment of light-viscosity to medium-viscosity oil-contaminated water, while further validation with crude oil or real industrial effluents is needed.

CRediT authorship contribution statement

Zhe Tang: Visualization, Validation, Methodology, Investigation, Formal analysis, Data curation, Conceptualization, Writing – original draft. **Oriol Rius-Ayra:** Writing – review and editing, Project administration, Resources, Software, Supervision.

Declaration of Competing Interest

The authors declare that they have no known competing financial interests or personal relationships that could have appeared to influence the work reported in this paper.

Acknowledgements

Zhe Tang acknowledges the financial support from the FI-SDUR predoctoral research fellowship. This work was supported by the FI-SDUR program of the Department of Research and Universities of the Generalitat de Catalunya, and co-financed by the European Social Fund Plus (Grant Reference Number: 2024 FISDU 00151). Dr. Oriol Rius-Ayra is a Serra Húnter Fellow.

Data Availability

View Article Online
DOI: 10.1039/D6MA00298F

Data will be made available on request.

References

[1] B.J. Singh, A. Chakraborty, R. Sehgal, A systematic review of industrial wastewater management: Evaluating challenges and enablers, J. Environ. Manage. 348 (2023). https://doi.org/10.1016/J.JENVMAN.2023.119230.

[2] X. Yu, X. He, Z. Qi, M. Yang, X. Li, D. Xiong, Interactions among microplastics, spilled oil and dispersant: Impacts of marine environmental conditions, Mar. Pollut. Bull. 222 (2026). https://doi.org/10.1016/J.MARPOLBUL.2025.118501.

[3] Z. Cai, M. Li, Z. Zhu, X. Wang, Y. Huang, T. Li, H. Gong, M. Yan, Biological Degradation of Plastics and Microplastics: A Recent Perspective on Associated Mechanisms and Influencing Factors, Microorganisms 11 (2023). https://doi.org/10.3390/MICROORGANISMS11071661.

[4] A.M.A. Pintor, V.J.P. Vilar, C.M.S. Botelho, R.A.R. Boaventura, Oil and grease removal from wastewaters: Sorption treatment as an alternative to state-of-the-art technologies. A critical review, Chem. Eng. J. 297 (2016) 229–255. https://doi.org/10.1016/J.CEJ.2016.03.121.

[5] P.D. Sutrisna, K.A. Kurnia, U.W.R. Siagian, S. Ismadji, I.G. Wenten, Membrane

View Article Online
DOI: 10.1039/D6MA00298F

fouling and fouling mitigation in oil–water separation: A review, J. Environ. Chem. Eng. 10 (2022). https://doi.org/10.1016/J.JECE.2022.107532.

[6] M.H. José, J.P. Canejo, M.H. Godinho, Oil/Water Mixtures and Emulsions Separation Methods—An Overview, Materials (Basel). 16 (2023). https://doi.org/10.3390/MA16062503.

[7] Y. Pan, S.H. Gao, C. Ge, Q. Gao, S. Huang, Y. Kang, G. Luo, Z. Zhang, L. Fan, Y. Zhu, A.J. Wang, Removing microplastics from aquatic environments: A critical review, Environ. Sci. Ecotechnology 13 (2023). https://doi.org/10.1016/J.ESE.2022.100222.

[8] O. Rius-Ayra, A. Biserova-Tahchieva, V. Sansa-López, N. Llorca-Isern, Superhydrophobic 304 Stainless Steel Mesh for the Removal of High-Density Polyethylene Microplastics, Langmuir 38 (2022) 5943–5953. https://doi.org/10.1021/ACS.LANGMUIR.2C00803.

[9] B. Bhushan, Y.C. Jung, Natural and biomimetic artificial surfaces for superhydrophobicity, self-cleaning, low adhesion, and drag reduction, Prog. Mater. Sci. 56 (2011) 1–108. https://doi.org/10.1016/J.PMATSCI.2010.04.003.

[10] X. Zhang, F. Shi, J. Niu, Y. Jiang, Z. Wang, Superhydrophobic surfaces: From structural control to functional application, J. Mater. Chem. 18 (2008) 621–633. https://doi.org/10.1039/B711226B.

View Article Online
DOI: 10.1039/D6MA00298F

[11] S.M.R. Razavi, J. Oh, S. Sett, L. Feng, X. Yan, M.J. Hoque, A. Liu, R.T. Haasch, M. Masoomi, R. Bagheri, N. Miljkovic, Superhydrophobic Surfaces Made from Naturally Derived Hydrophobic Materials, ACS Sustain. Chem. Eng. 5 (2017) 11362–11370. https://doi.org/10.1021/ACSSUSCHEMENG.7B02424.

[12] C. Schlaich, L. Yu, L. Cuellar Camacho, Q. Wei, R. Haag, Fluorine-free superwetting systems: Construction of environmentally friendly superhydrophilic, superhydrophobic, and slippery surfaces on various substrates, Polym. Chem. 7 (2016) 7446–7454. https://doi.org/10.1039/C6PY01596D.

[13] Z. Xu, Y. Zhao, H. Wang, H. Zhou, C. Qin, X. Wang, T. Lin, Fluorine-Free Superhydrophobic Coatings with pH-induced Wettability Transition for Controllable Oil-Water Separation, ACS Appl. Mater. Interfaces 8 (2016) 5661–5667. https://doi.org/10.1021/ACSAMI.5B11720.

[14] O. Rius-Ayra, A. Biserova-Tahchieva, I. López-Jiménez, N. Llorca-Isern, Superhydrophobic and nanostructured CuFeCo powder alloy for the capture of microplastics, Colloids Surfaces A Physicochem. Eng. Asp. 627 (2021). https://doi.org/10.1016/J.COLSURFA.2021.127075.

[15] Z. Wang, Q. Li, Z. She, F. Chen, L. Li, Low-cost and large-scale fabrication method for an environmentally-friendly superhydrophobic coating on magnesium alloy, J. Mater. Chem. 22 (2012) 4097–4105. https://doi.org/10.1039/C2JM14475A.

View Article Online
DOI: 10.1039/D6MA00298F

[16] R.S. Sutar, S.S. Latthe, A.R. Jundle, P.P. Gaikwad, S.S. Ingole, S. Nagappan, Y.H. Kim, A.K. Bhosale, V.S. Saji, S. Liu, A facile approach for oil-water separation using superhydrophobic polystyrene-silica coated stainless steel mesh bucket, Mar. Pollut. Bull. 198 (2024). https://doi.org/10.1016/J.MARPOLBUL.2023.115790.

[17] C. Chen, X. Zhu, B. Chen, Durable Superhydrophobic/Superoleophilic Graphene-Based Foam for High-Efficiency Oil Spill Cleanups and Recovery, Environ. Sci. Technol. 53 (2019) 1509–1517. https://doi.org/10.1021/ACS.EST.8B04642.

[18] H. Shayesteh, M.S. Khosrowshahi, H. Mashhadimoslem, F. Maleki, Y. Rabbani, H.B.M. Emrooz, Durable superhydrophobic/superoleophilic melamine foam based on biomass-derived porous carbon and multi-walled carbon nanotube for oil/water separation, Sci. Rep. 13 (2023) 4515. https://doi.org/10.1038/S41598-023-31770-X.

[19] F. Asjadi, M. Yaghoobi, Facile and scalable preparation of superhydrophobic brass mesh for efficient and rapid separation of oil and water, Sci. Rep. 14 (2024). https://doi.org/10.1038/S41598-024-63428-7.

[20] Y. Liu, Z. Lin, Y. Luo, R. Wu, R. Fang, A. Umar, Z. Zhang, Z. Zhao, J. Yao, S. Zhao, Superhydrophobic MOF based materials and their applications for oil-water separation, J. Clean. Prod. 420 (2023). https://doi.org/10.1016/J.JCLEPRO.2023.138347.

[21] H. Sun, Z. Liu, K. Liu, M.E. Gibril, F. Kong, S. Wang, Lignin-based superhydrophobic melamine resin sponges and their application in oil/water separation, Ind. Crops Prod.

View Article Online
DOI: 10.1039/D6MA00298F

170 (2021). https://doi.org/10.1016/J.INDCROP.2021.113798.

[22] J. He, J. He, M. Yuan, M. Xue, X. Ma, L. Hou, T. Zhang, X. Liu, M. Qu, Facile Fabrication of Eco-Friendly Durable Superhydrophobic Material from Eggshell with Oil/Water Separation Property, Adv. Eng. Mater. 20 (2018). https://doi.org/10.1002/ADEM.201701180.

[23] S. Fan, L. Tang, X. Zhao, G. Xu, W. Fan, Facile Preparation of Durable Superhydrophobic Coating by Liquid-Phase Deposition for Versatile Oil/Water Separation, Coatings 13 (2023). https://doi.org/10.3390/COATINGS13050925.

[24] M. He, S. Wu, S. Xiong, L. Zhang, C. Lai, X. Peng, S. Zhong, Z.H. Lu, S. Chen, W.G. Zhang, C. Tan, G. Peng, C. Liu, Hydrophobic Carbon Nitride Nanolayer Enables High-Flux Oil/Water Separation with Photocatalytic Antifouling Ability, Nano Lett. 23 (2023) 10563–10570. https://doi.org/10.1021/ACS.NANOLETT.3C03482.

[25] O. Rius-Ayra, A. Ren, A. Biserova-Tahchieva, Superhydrophobic Materials and Intermolecular Forces for Microplastics Removal, ACS Mater. Lett. 7 (2025) 1723–1731. https://doi.org/10.1021/acsmaterialslett.4c02655.

[26] A. Ren, O. Rius-Ayra, M. Kang, N. Llorca-Isern, Mechanically robust superhydrophobic coatings for efficiency and recyclable microplastic removal, Prog. Org. Coatings 205 (2025). https://doi.org/10.1016/j.porgcoat.2025.109328.

View Article Online
DOI: 10.1039/D6MA00298F

[27] A. Ren, O. Rius-Ayra, M. Kang, N. Llorca-Isern, Durably Superhydrophobic Magnetic Cobalt Ferrites for Highly Efficient Oil-Water Separation and Fast Microplastic Removal, Langmuir 40 (2024) 21533–21546. https://doi.org/10.1021/acs.langmuir.4c02420.

[28] Y. Zhang, X. Yang, S. Wang, J. Liu, X. Liu, K. Chan, J. Liu, Multifunctional superhydrophobic copper mesh for efficient oil/water separation and fog collection, Colloids Surfaces A Physicochem. Eng. Asp. 657 (2023) 130603. https://doi.org/10.1016/J.COLSURFA.2022.130603.

[29] F. Zhang, R. Wu, H. Zhang, Y. Ye, Z. Chen, A. Zhang, Novel Superhydrophobic Copper Mesh-Based Centrifugal Device for Edible Oil–Water Separation, ACS Omega 9 (2024) 16303–16310. https://doi.org/10.1021/ACSOMEGA.3C10436.

[30] S. Gao, X. Dong, J. Huang, J. Dong, Y. Cheng, Z. Chen, Y. Lai, Co-solvent induced self-roughness superhydrophobic coatings with self-healing property for versatile oil-water separation, Appl. Surf. Sci. 459 (2018) 512–519. https://doi.org/10.1016/J.APSUSC.2018.08.041.

[31] S. Gao, X. Dong, J. Huang, S. Li, Y. Li, Z. Chen, Y. Lai, Rational construction of highly transparent superhydrophobic coatings based on a non-particle, fluorine-free and water-rich system for versatile oil-water separation, Chem. Eng. J. 333 (2018) 621–629. https://doi.org/10.1016/J.CEJ.2017.10.006.

View Article Online
DOI: 10.1039/D6MA00298F

[32] S. Men, X. Jiang, X. Xiang, G. Sun, Y. Yan, Z. Lyu, Y. Jin, Synthesis of Cellulose Long-Chain Esters in 1-Butyl-3-methylimidazolium Acetate: Structure-Property Relations, Polym. Sci. - Ser. B 60 (2018) 349–353. https://doi.org/10.1134/S1560090418030144.

[33] S. Hadaoui, H. Liu, Z. Lei, S. Lebègue, R. Benbalagh, A. Courty, A. Naitabdi, Zinc oxide-copper model nanocatalysts for CO2 hydrogenation: morphology and interface effects, Mater. Adv. 5 (2023) 1251–1263. https://doi.org/10.1039/D3MA00872J.

[34] Alghunaimi, Hydrophobic stainless-steel copper-coated mesh and method of synthesizing same, (2019).

[35] Q.T. Trinh, K. Bhola, P.N. Amaniampong, F. Jérôme, S.H. Mushrif, Synergistic Application of XPS and DFT to Investigate Metal Oxide Surface Catalysis, J. Phys. Chem. C 122 (2018) 22397–22406. https://doi.org/10.1021/ACS.JPCC.8B05499.

[36] D. V. Sivkov, O. V. Petrova, S. V. Nekipelov, A.S. Vinogradov, R.N. Skandakov, S.I. Isaenko, A.M. Ob'edkov, B.S. Kaverin, I. V. Vilkov, R.I. Korolev, V.N. Sivkov, The identification of cu–o–c bond in cu/mwcnts hybrid nanocomposite by xps and nexafs spectroscopy, Nanomaterials 11 (2021). https://doi.org/10.3390/NANO11112993/S1.

[37] T.M. Ivanova, K.I. Maslakov, A.A. Sidorov, M.A. Kiskin, R. V. Linko, S. V. Savilov, V. V. Lunin, I.L. Eremenko, XPS detection of unusual Cu(II) to Cu(I) transition on the surface of complexes with redox-active ligands, J. Electron Spectros. Relat. Phenomena

View Article Online
DOI: 10.1039/D6MA00298F

238 (2020) 146878. https://doi.org/10.1016/J.ELSPEC.2019.06.010.

[38] R. Ma, R. Li, Q. Niu, Y. Zeng, J. Li, S. Bai, Y. Cheng, Preparation of Superhydrophobic Surfaces Based on Copper Mesh Substrates and Its Application Performance, ACS Omega 8 (2023) 45616–45625. https://doi.org/10.1021/ACSOMEGA.3C05834.

[39] R. Huang, L. Wang, Y. Lin, Y. Dong, D. You, Surface modification of carbonyl iron powders with silicone polymers in supercritical fluid to get higher dispersibility and higher thermal stability, Surf. Interface Anal. 49 (2017) 79–84. https://doi.org/10.1002/SIA.6061;ISSUE:ISSUE:DOI.

[40] X. Su, H. Li, X. Lai, L. Zhang, J. Wang, X. Liao, X. Zeng, Vapor-Liquid Sol-Gel Approach to Fabricating Highly Durable and Robust Superhydrophobic Polydimethylsiloxane@Silica Surface on Polyester Textile for Oil-Water Separation, ACS Appl. Mater. Interfaces 9 (2017) 28089–28099. https://doi.org/10.1021/ACSAMI.7B08920.

[41] X. Su, H. Li, X. Lai, L. Zhang, T. Liang, Y. Feng, X. Zeng, Polydimethylsiloxane-based superhydrophobic surfaces on steel substrate: Fabrication, reversibly extreme wettability and oil-water separation, ACS Appl. Mater. Interfaces 9 (2017) 3131–3141. https://doi.org/10.1021/ACSAMI.6B13901.

[42] A.M. Rather, U. Manna, Stretchable and durable superhydrophobicity that acts both in air and under oil, J. Mater. Chem. A 5 (2017) 15208–15216.

View Article Online
DOI: 10.1039/D6MA00298F

https://doi.org/10.1039/C7TA04073C.

[43] Y. Chen, Y. Xue, S. Ma, H. Shi, Y. Wang, H. Ren, K. Xu, Enhanced oil/water separation using superhydrophobic nano SiO2-modified porous melamine sponges, Chemosphere 369 (2024). https://doi.org/10.1016/J.CHEMOSPHERE.2024.143879.

[44] C. Wang, W. Xiao, Q. Li, X. Tian, J. Xu, K. Ding, Oil removal from wastewater with biomass-derived hydrochars laboratory insights, Sci. Rep. 15 (2025). https://doi.org/10.1038/S41598-025-07240-X.

[45] Y. Ma, M. Maihaiti, M. Mamat, S. Feng, Oil-water separation via superhydrophilic materials: Fundamentals and perspectives for 2D/3D system design, J. Environ. Chem. Eng. 13 (2025). https://doi.org/10.1016/J.JECE.2025.119564.

[46] J. Jiang, S. Wan, C. Wen, L. Tang, N. Xu, Frontiers in Innovative Materials and Technologies for Oil–Water Separation, Polymers (Basel). 17 (2025). https://doi.org/10.3390/POLYM17121635.

[47] Y. Liu, K. Liu, W. Zhao, J. Liu, J. Hua, Swan feather-spired fluorine-free superhydrophobic self-cleaning cotton cloth with strong oil-water separation function, Prog. Org. Coatings 183 (2023). https://doi.org/10.1016/J.PORGCOAT.2023.107798.

[48] Z. Chu, Y. Feng, S. Seeger, Oil/water separation with selective superantiwetting/superwetting surface materials, Angew. Chemie - Int. Ed. 54 (2015)

View Article Online
DOI: 10.1039/D6MA00298F

2328–2338. https://doi.org/10.1002/ANIE.201405785.

[49] Y. Yang, E. Huang, P. Dansawad, Y. Li, Y. Qing, C. Lv, L. Cao, S. You, Y. Li, W. Li, Superhydrophilic and underwater superoleophobic PVDF-PES nanofibrous membranes for highly efficient surfactant-stabilized oil-in-water emulsions separation, J. Memb. Sci. 687 (2023). https://doi.org/10.1016/J.MEMSCI.2023.122044.

[50] B. Wang, S. Handschuh-Wang, J. Shen, X. Zhou, Z. Guo, W. Liu, M. Pumera, L. Zhang, Small-Scale Robotics with Tailored Wettability, Adv. Mater. 35 (2023). https://doi.org/10.1002/ADMA.202205732.

[51] K. Liu, M. Sorgato, E. Savio, From Hydrophilic to Superhydrophobic: Tuning Surface Wettability through Salvinia-Inspired Topographies, ACS Appl. Mater. Interfaces 17 (2025) 45066–45081. https://doi.org/10.1021/ACSAMI.5C07461.

[52] O. Rius-Ayra, A. Biserova-Tahchieva, N. Llorca-Isern, Removal of dyes, oils, alcohols, heavy metals and microplastics from water with superhydrophobic materials, Chemosphere 311 (2023). https://doi.org/10.1016/J.CHEMOSPHERE.2022.137148.

[53] Y. Zhao, Z. Xu, L. Gong, S. Yang, H. Zeng, C. He, D. Ge, L. Yang, Recoverable underwater superhydrophobicity from a fully wetted state via dynamic air spreading, IScience 24 (2021). https://doi.org/10.1016/J.ISCI.2021.103427.

[54] X. Jiang, B. Liu, Q. Zeng, F. Yang, Z. Guo, Mussel-Inspired Robust Peony-like

View Article Online
DOI: 10.1039/D6MA00298F

Cu3(PO4)2 Composite Switchable Superhydrophobic Surfaces for Bidirectional Efficient Oil/Water Separation, ACS Appl. Mater. Interfaces 15 (2023) 13700–13710. https://doi.org/10.1021/ACSAMI.2C21151.

[55] X. Hu, T. Xing, H. Wu, K. Wei, M. Souare, C. Dong, Separation Principles and Strategies for an Oil–Water Separation Membrane with Special Wettability, Membranes (Basel). 15 (2025). https://doi.org/10.3390/MEMBRANES15080241.

[56] X. Zhang, C. Hu, H. Xiang, Z. Xu, C. Huang, H. Yin, T. Li, K. Ren, Preparation of robust superhydrophobic stainless steel mesh for Oil-Water separation through Mn-Assisted control of one-step electrodeposited Zn growth, Chem. Eng. J. 498 (2024). https://doi.org/10.1016/J.CEJ.2024.155369.

[57] S. Rasouli, N. Rezaei, H. Hamedi, S. Zendehboudi, X. Duan, Superhydrophobic and superoleophilic membranes for oil-water separation application: A comprehensive review, Mater. Des. 204 (2021). https://doi.org/10.1016/J.MATDES.2021.109599.

[58] M. Qasim, A. Ali, A. Alnaser, Micropatterned superhydrophobic meshes coated with low-cost carbon nanoparticles for efficient oil/water separation, RSC Adv. 14 (2024) 20426–20440. https://doi.org/10.1039/D4RA03275F.

[59] Y. Wang, P. Liu, R. Luo, B. Chen, J. Li, F. Yang, H. Zhou, J. Zeng, L. Xing, J. Guo, Design and fabrication of superhydrophobic photothermal coating on copper mesh and its applications on anti-corrosion, anti-icing and oil-water separation, Prog. Org.

View Article Online
DOI: 10.1039/D6MA00298F

Coatings 188 (2024). https://doi.org/10.1016/J.PORGCOAT.2024.108243.

[60] B. Xiang, J. Gong, Y. Sun, W. Yan, R. Jin, J. Li, High permeability PEG/MXene@MOF membrane with stable interlayer spacing and efficient fouling resistance for continuous oily wastewater purification, J. Memb. Sci. 691 (2024) 122247. https://doi.org/10.1016/j.memsci.2023.122247.

[61] J. Gong, B. Xiang, R. Jin, Z. Li, W. Liu, J. Li, Robust peony-like Cu3(PO4)2/UiO-66-NH2/PVA membranes with exceptional anti-fouling performance for high flux emulsion separation, Sep. Purif. Technol. 379 (2025) 134915. https://doi.org/10.1016/j.seppur.2025.134915.

[62] J. Liu, J. He, P. Wu, C. Yang, W. Jiang, Controllable superwettability of Cu mesh by one-step immersion in fatty acids with different carbon chain lengths, Surf. Coatings Technol. 396 (2020). https://doi.org/10.1016/J.SURFCOAT.2020.125934.

[63] P. Shen, N. Uesawa, S. Inasawa, Y. Yamaguchi, Characterization of flowerlike silicon particles obtained from chemical etching: Visible fluorescence and superhydrophobicity, Langmuir 26 (2010) 13522–13527. https://doi.org/10.1021/LA102516G.

[64] Q. Tong, Z. Fan, B. Wang, Q. Liu, Y. Bo, L. Qian, Preparation and Application of Superhydrophobic Copper Mesh by Chemical Etching and In-situ Growth, Front. Chem. 9 (2021). https://doi.org/10.3389/FCHEM.2021.737550.

View Article Online
DOI: 10.1039/D6MA00298F

[65] Y.C. Sang, A.B. Albadarin, A.H. Al-Muhtaseb, C. Mangwandi, J.N. McCracken, S.E.J. Bell, G.M. Walker, Properties of super-hydrophobic copper and stainless steel meshes: Applications in controllable water permeation and organic solvents/water separation, Appl. Surf. Sci. 335 (2015) 107–114. https://doi.org/10.1016/J.APSUSC.2015.02.034.

[66] A. Al Harraq, B. Bharti, Microplastics through the Lens of Colloid Science, ACS Environ. Au 2 (2022) 3–10. https://doi.org/10.1021/ACSENVIRONAU.1C00016.

[67] L. Fu, J. Li, G. Wang, Y. Luan, W. Dai, Adsorption behavior of organic pollutants on microplastics, Ecotoxicol. Environ. Saf. 217 (2021). https://doi.org/10.1016/J.ECOENV.2021.112207.

[68] X. Gong, S. Luo, Y. Yang, Q. Zhou, Fe(III) Adsorption onto Microplastics in Aquatic Environments: Interaction Mechanism, Influencing Factors, and Adsorption Capacity Prediction, Water (Switzerland) 17 (2025). https://doi.org/10.3390/W17091316.

[69] M.A.H. Bhuyan, R. Busquets, L.C. Campos, T. Luukkonen, Separation of microplastics from water using superhydrophobic silane-coupling-agent-modified geopolymer foam, Sep. Purif. Technol. 339 (2024). https://doi.org/10.1016/J.SEPPUR.2024.126709.

[70] C. Yang, Y. Wang, H. Fu, S. Yang, Y. Zhu, H. Yue, W. Jiang, B. Liang, A stable eco-friendly superhydrophobic/superoleophilic copper mesh fabricated by one-step immersion for efficient oil/water separation, Surf. Coatings Technol. 359 (2019) 108–116. https://doi.org/10.1016/J.SURFCOAT.2018.12.037.

View Article Online
DOI: 10.1039/D6MA00298F

View Article Online
DOI: 10.1039/D6MA00298F

Data availability statement

Data for this article, including the used photos of the article 3D-Printed Superhydrophobic Copper Mesh for Oil/Water Separation and Microplastics Capture are available at Mendeley Data at https://doi.org/10.17632/y2sxpcpwxf.1.